Front. Mater. Sci. 2016, 10(1): 56–65
DOI 10.1007/s11706-016-0320-5

RESEARCH ARTICLE

Properties of poly(1-naphthylamine)/Fe_3O_4 composites and arsenic adsorption capacity in wastewater

Minh Thi TRAN (✉)[1], Thi Huyen Trang NGUYEN[1], Quoc Trung VU[2], and Minh Vuong NGUYEN[3]

1 Faculty of Physics, Hanoi National University of Education, 136-Xuanthuy Street, Caugiay District, Hanoi, Vietnam
2 Faculty of Chemistry, Hanoi National University of Education, 136-Xuanthuy Street, Caugiay District, Hanoi, Vietnam
3 Department of Physics, Quynhon University, 170 An Duong Vuong, Quynhon, Vietnam

© Higher Education Press and Springer-Verlag Berlin Heidelberg 2016

ABSTRACT: The research results of poly(1-naphthylamine)/Fe_3O_4 (PNA/Fe_3O_4) nanocomposites synthesized by a chemical method for As(III) wastewater treatment are presented in this paper. XRD patterns and TEM images showed that the Fe_3O_4 grain size varied from 13 to 20 nm. The results of Raman spectral analysis showed that PNA participated in part of the PNA/Fe_3O_4 composite samples. The grain size of PNA/Fe_3O_4 composite samples is about 25–30 nm measured by SEM. The results of vibrating sample magnetometer measurements at room temperature showed that the saturation magnetic moment of PNA/Fe_3O_4 samples decreased from 63.13 to 43.43 emu/g, while the PNA concentration increased from 5% to 15%. The nitrogen adsorption–desorption isotherm of samples at 77 K at a relative pressure P/P_0 of about 1 was studied in order to investigate the surface and porous structure of nanoparticles by the BET method. Although the saturation magnetic moments of samples decreased with the polymer concentration increase, the arsenic adsorption capacity of the PNA/Fe_3O_4 sample with the PNA concentration of 5% is better than that of Fe_3O_4 in a solution with pH = 7. In the solution with pH > 14, the arsenic adsorption of magnetic nanoparticles is insignificant.

KEYWORDS: poly(1-naphthylamin)/Fe_3O_4 nanocomposite; magnetization; arsenic adsorption

Contents

Received June 30, 2015; accepted October 26, 2015

E-mail: tranminhthi@hnue.edu.vn

1 Introduction

Transition metal-doped Fe_3O_4 magnetic nanomaterials are attractive [1–5] because they have applications in many fields: information storage, ink, arsenic [6–10], heavy metal treatment [11–13], cancer treatment and dye pollution treatment in the wastewater [14–16]. Magnetic nanoparticles express many special properties when their specific surface areas increase. Various metal oxide heterostructures, such as meso-porous Al_2O_3, TiO_2, CuO, ZrO_2 and MnO_2 [1,17–23], have been investigated for the removal of Cd, Cr and As. However, using these oxides for arsenic absorption faces problems in recovering from aqueous solutions and leaving residuals in the solution. Recently, researchers studied the possibility of magnetic nanoporous materials as the arsenic absorbent. These magnetic nanoporous materials bearing adsorbed arsenic can be conveniently separated from aqueous solutions with the assistance of an external magnetic field. It is believed that the nanosized ferrites can exhibit improved physical and chemical properties and hence can effectively be used for various applications. At present, researchers are interested in the chemical instability and the decrease of saturate magnetic moment of Fe_3O_4 over time and their effectiveness in application [10,19,24–29].

In order to stabilize the chemical properties of materials, Fe_3O_4 was doped with some transition metals. In terms of Fe_3O_4 crystal structure, the unit cell of spinel ferrite (AB_2O_4) consists of cubic closed-packed arrays of oxygen ions which result in two kinds of interstitial sites denoted as tetrahedral A-site (Fe^{3+}) and octahedral B-site ($n(Fe^{2+})$: $n(Fe^{3+})$ = 1:1) [19,25]. In the work reported by Ref. [26], the magnetization of $Ni_{1-x}Zn_xFe_2O_4$ samples (x = 0, 0.5 and 1) was changed by substitutions of Ni^{2+} ions into A-sites and B-sites, meanwhile the substitution of Zn^{2+} ions into a preferential site for A-sites. Thus, the increasing content of nonmagnetic Zn^{2+} ions into A-sites caused strong decrease of the saturation magnetization of $Ni_{1-x}Zn_xFe_2O_4$ samples when x is close to 1 [26]. Besides, the $Ni_{0.5}Zn_{0.5}Fe_2O_4$ sample [10] with the saturation magnetic moment of 46.1 emu/g and the specific surface area of 49.0 m^2/g achieved the arsenic equilibrium adsorption quantity of 7.2 mg/g when the initial arsenic concentration reaches 3 mg/L.

Recently, the composite materials of iron oxide-coated sand (IOCS) and iron oxide-coated diatomite (IOCD) [30–31] were investigated on the influential factor to remove arsenic. Some papers presented on the application of poly-(1-naphthylamine) (PNA) in sensitive ethanol chemical sensor and PNA/ZnO nanocomposites in degradation of methylene blue dye [32–33]. However, there is not any announcement about the arsenic adsorbed capacity of polymer/Fe_3O_4 nanocomposite materials. In this report, we present our research results about the synthesis, magnetic properties, microstructure of PNA/Fe_3O_4 nanocomposite materials and the influence of PNA concentration to the arsenic adsorbed capacity in water at different pH values. Due to the nature that the adsorption process was attributed to the inelastic exchange interaction energy between the arsenic and the porous materials with high specific surface area of adsorption substance, parameters of the arsenic adsorption isotherm process are studied and calculated using the Langmuir isotherm equation [6,10,17].

2 Experimental

The high-purity initial chemicals from Merck Chemical Company were used: $FeCl_3 \cdot 6H_2O$; Na_2SO_3; acetone with 99% purity; the solutions: NH_3 with concentration of 25 mol.% and the original AsO_3 solution with the arsenic concentration of 1 g/L (1 g/L = 10^6 ppb corresponding to 10^5 times higher than that allowed arsenic level of 10 ppb regulated by the World Health Organization (WHO), European Commission (EC) and United States Environmental Protection Agency (US EPA)). Besides, the NaOH and HCl solutions were also used to adjust the pH of solution.

2.1 Synthesis of Fe_3O_4

The $FeCl_3 \cdot 6H_2O$ solution containing Fe^{3+} was mixed with a Na_2SO_3 solution. These mixed solutions were stirred until they turned to yellow in color. Then the NH_3 solution was added dripping slowly, drop by drop, until pH = 10. The solution with black color was obtained after it was stirred for 30 min. The magnetic materials were obtained by using magnets, and then passed through a filter. These powders were dried at 50°C in low-pressure conditions for 48 h. These dried products was finely ground that called Fe_3O_4 nanoparticles. Chemical reactions occur in the synthesized process as follows:

$$2FeCl_3 + Na_2SO_3 + H_2O \rightarrow 2FeCl_2 + Na_2SO_4 + 2HCl \quad (1)$$

$$2FeCl_3 + FeCl_2 + 8NH_3 + 4H_2O \rightarrow Fe_3O_4\downarrow + 8NH_4Cl \quad (2)$$

2.2 Synthesis of PNA/Fe_3O_4 nanocomposites

Synthesis of PNA/Fe_3O_4 nanocomposites by the polymerization method takes place according to the following steps:

1) The exact amount of Fe_3O_4 was taken into 100 mL of distilled water. Adding 40 mL of isopropanol and $C_{10}H_9N$ naphthylamine, respectively, and stirred strongly for 1 h.

2) Then the amount of $(NH_4)_2S_2O_8$ solution was added dripping slowly, drop by drop, in which the molar ratio between the $C_{10}H_9N$ monomer and the $(NH_4)_2S_2O_8$ oxidizing agent is 1:1.5. These black-blue mixed solutions were stirring for 2 h with exothermal reaction.

3) The powders were filtered and then were dried by Labconco freeze concentration apparatus (USA) for 5 h with the pressure of 1 mPa at −40°C temperature.

In this topic, Fe_3O_4, PNA (M_0) and PNA/Fe_3O_4 nanocomposite powders (forming with the PNA mass ratio of 5%, 10% and 15% are signed as M_1, M_2 and M_3, respectively) are shown in Table 1.

Table 1 Compositions of Fe_3O_4, M_0, M_1, M_2 and M_3 samples

Sample	Weight /g	
	Fe_3O_4	PNA
Fe_3O_4	20	0
M_0	0	3.0
M_1	20	1.0
M_2	20	2.0
M_3	20	3.0

The microstructure of the samples was measured by X-ray diffraction (XRD, D5005, Bruker), transmission electron microscopy (TEM, JEOL 5410 TEM NV) and scanning electron microscopy (SEM, S4800-NIHE) measurements. Their magnetic properties were measured using a vibrating sample magnetometer (VSM). The mesopore structure of samples was measured by the Brunauer–Emmett–Teller (BET) method using TriStar 3000 V6.07A instrument with TriStar 3000 V6.08 software.

Raman scattering investigations at the 633 nm wavelength with the laser beam energy of 3 mW were performed on the Ramanlog 9I (USA) equipment. The obtained powders were mixed into an As(III) solution with an arsenic concentration of about 10^5 times higher than the allowed level and stirred for 20 min. In order to determine the saturated adsorption capacity of the material, the arsenic concentrations in the solution before and after stirring were measured using atomic absorption spectroscopy (AAS, 6300 Shimadzu).

3 Results and discussion

3.1 Microstructure properties

Figure 1 shows the XRD patterns of Fe_3O_4 and M_1 samples in which diffraction peaks coincide with the standard spectrum in the Roentgen diffraction pattern. Therefore, these samples are single phase with the cubic structure of centered face. The diffraction pattern of polymer-coated Fe_3O_4 sample (M_1) completely is the same of Fe_3O_4 sample, so this issue proves that the coated polymers do not affect the crystal structure of Fe_3O_4. The lattice constants of the Fe_3O_4 and M_1 samples were calculated from the Bragg diffraction condition $2d\sin\theta = n\lambda$ by the equation: $a = d_{hkl}\sqrt{h^2 + k^2 + l^2}$, where d_{hkl} is the distance between the lattice planes. Using the Debye–Scherrer formula $D = 0.9\lambda/(\beta\cos\theta)$ (here, λ is the wavelength of line Cu Kα (1.5416 Å), β is the full width at haft maximum and θ is the diffraction angle), the particle sizes were calculated for Fe_3O_4 and M_1 samples. By this ways, the lattice constant values and particle sizes of the samples seem no difference between Fe_3O_4 and M_1 samples. The calculated values of lattice constant and the particle size are 8.376 Å and 14.49 nm, respectively, for these samples.

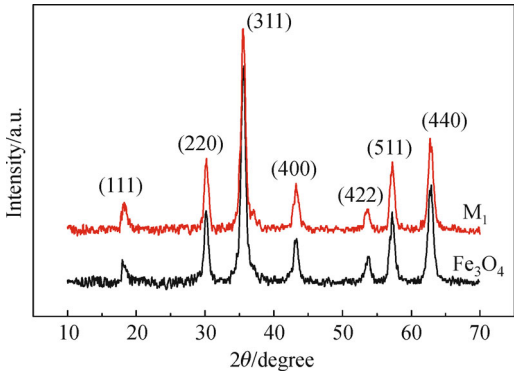

Fig. 1 XRD patterns of Fe_3O_4 and M_1.

Image TEM in Fig. 2 shown the agglomerate of nanocomposite grains in M_3 sample with sizes from 13 to 20 nm. As PNA polymers are of the amorphous materials, the particle size for M_1 sample could be calculated by the Debye–Scherrer equation of about 14.49 nm that is the size of the core Fe_3O_4 crystal structure.

Thus, the size results from the TEM image are lager than that from the XRD pattern of samples, and these results are consistent and demonstrate the shell–core structures of the material nanocomposite.

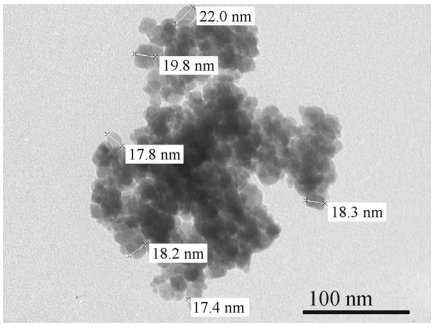

Fig. 2 TEM image of M_3.

The SEM images (see Fig. 3) also show that the nanocomposite particles of about 25–30 nm have high uniformity and were created by covering the polymer the outside of Fe_3O_4 particles.

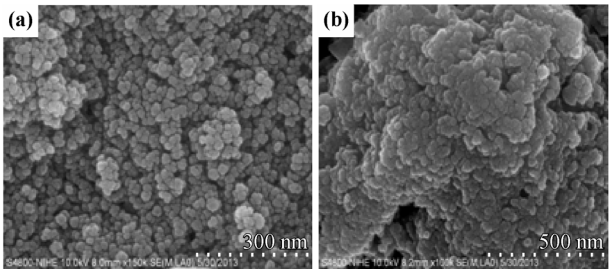

Fig. 3 SEM images of PNA/Fe_3O_4: **(a)** M_1; **(b)** M_2.

The inset of Fig. 4(a) shows Ramman spectrum of Fe_3O_4 with two small peaks at the wavenumbers 360 and 666 cm^{-1}. Meanwhile, Ramman spectra of M_0 (PNA) and M_3 samples (two curves in Fig. 4(a)) show the characteristic peaks of PNA in samples, in which the 1495 and 1547.8 cm^{-1} peaks of M_3 with stronger intensity are very close to the 1446–1492 and 1571 cm^{-1} peaks of PNA nanoglobules [32]. This range is characteristic the valence oscillation of C = C group, the C = N chemotherapy group, and the N – H, C – H, C – C groups. The 1359.55 cm^{-1} peak is close to the Raman shift of 1351 cm^{-1} [32] assigned to $C-N^+$ stretching modes of delocalized polaronic charge carriers. In addition, the 1149.96 cm^{-1} peak of M_3 sample is also very close to the Raman shift at 1154 cm^{-1} of PNA [32] that is corresponding to the oscillation frequency of the C – C stretching/C – H plane bending group. Thus, the results of Raman spectral analysis showed that the PNA with the structure in Fig. 4(b) participated in part of the composite samples and it expressed the oxidation state with the oscillation groups of υ_{C-N}, υ_{C-N^+} and δ_{C-H}.

These results demonstrate that the nanocomposite grains were formed by polymerization of monomers on the surface of metal oxide particles.

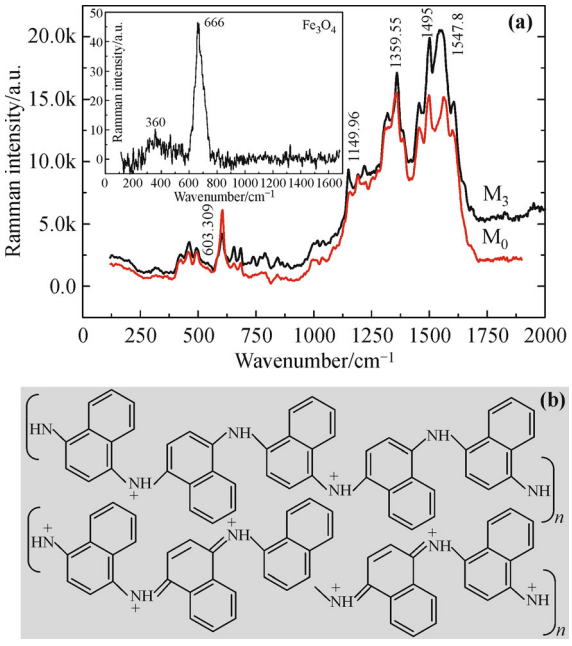

Fig. 4 **(a)** Ramman spectra of M_3 (PNA/Fe_3O_4) sample and M_0 (PNA) sample (inset: Fe_3O_4 sample). **(b)** PNA structure.

3.2 Magnetic and chemical instability of Fe_3O_4 sample

First, the stability of magnetic, microstructure property of Fe_3O_4 was investigated by examining a sample right after synthesized and that sample after 2 months. Curves a and b in Fig. 5 showed that the saturate magnetic moment of Fe_3O_4 sample decreased from 63.13 to 56 emu/g, corresponding to freshly synthesized sample and this sample measured after 2 months of synthesis. This decrease was attributed that after formation, Fe_3O_4 material is easy to be oxidized into γ-Fe_2O_3 due to the effects of oxygen in air as following equation:

$$4Fe_3O_4 + O_2 \rightarrow 6Fe_2O_3 \quad (3)$$

The appearance of γ-Fe_2O_3 phase can be seen in Raman spectra of Fe_3O_4 sample freshly synthesized and after 2 months (see the inset in Fig. 5). In the Raman spectrum of the pristine sample (curve a in Fig. 5), a peak with the wavenumber of 668 cm^{-1} can be observed corresponding to the A_{1g} oscillation mode of Fe_3O_4. In addition, the peak at 360 cm^{-1} with small intensity can also be detected which was attributed to the presence of the γ-Fe_2O_3 phase with such a tiny amount that it could not be detected by the XRD measurement. The appearance of the γ-Fe_2O_3 phase in the pristine sample might originate from the synthesis process in which the oxidation of Fe^{2+} into Fe^{3+} happened because

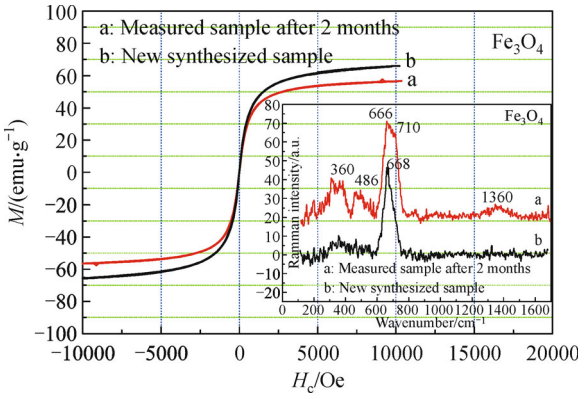

Fig. 5 Magnetic moment of Fe_3O_4: measured sample after 2 months (a); new synthesized sample (b). (Inset: Ramman spectra).

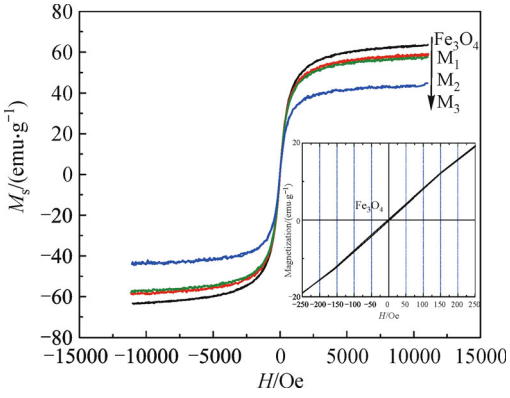

Fig. 6 Magnetic moment of samples (inset: the superparamagnetic properties with small H_c).

the samples were synthesized in the atmosphere. On the other hand, for the Raman spectrum of the 2 month-old Fe_3O_4 sample, peaks at 360, 486 and 1360 cm^{-1} corresponding to A_{1g} oscillation modes of γ-Fe_2O_3 were observed. Also, the 668 cm^{-1} peak of the spectrum in the inset of Fig. 5 showed signs of splitting into two peaks at 666 and 710 cm^{-1}. The appearance of additional peaks suggested that Fe_3O_4 is easy to be oxidized to form γ-Fe_2O_3. The change of magnetic moment and the chemical instability of the Fe_3O_4 sample might lead to the unexpected phenomena affecting to their application ability.

3.3 Magnetic properties of Fe_3O_4 and PNA/Fe_3O_4

Due to Fe_3O_4 is easy to be oxidized in atmosphere to form γ-Fe_2O_3. Thus, the coating of Fe_3O_4 nanoparticles by PNA polymer is the optimal solution to stabilize magnetic and chemical properties of samples.

The magnetization curves of Fe_3O_4, M_1, M_2 and M_3 samples (Fig. 6) expressed the super-paramagnetic properties with H_c value of about 3 Oe (sample Fe_3O_4 at the inset of Fig. 6). As shown in Table 2, the M_0 sample is of the non-magnetic material. Thus the magnetic moment of PNA/Fe_3O_4 decreased from 63.13 to 43.43 emu/g with the increase of the PNA concentration from 5% to 15%. However, the polymer shell contributed to the chemical stabilization of Fe_3O_4 cores, so the magnetic moment of samples is stable over time.

3.4 Arsenic adsorption capacity

In order to evaluate the arsenic adsorption capacity of Fe_3O_4, M_1, M_2 and M_3 samples, all the studies of the influence of polymer concentration, pH, and adsorption equilibrium time on the arsenic adsorption capacity were carried out at room temperature. For each measurement, the concentration of the original As(III) solution was fixed at 10^6 ppb (10^5 times higher than the permitted level by the WHO). Each adsorbent of Fe_3O_4, M_1, M_2 and M_3 with the mass of 0.01 g was put into the original arsenic solution. Then the mixture solution was stirred for 20 min for all samples. In these adsorption isotherms, the arsenic concentrations in the solutions before and after adsorption were measured by AAS.

3.4.1 Investigation of the effects of pH on the arsenic adsorption

The influence of pH level on the arsenic adsorption capacity of adsorbent materials was investigated shown in Fig. 7 for Fe_3O_4, M_1, M_2 and M_3 powders. These adsorbent materials of 0.01 g were used to adsorb arsenic in 100 mL solutions with the initial arsenic concentrations at different pH levels from 1 to 14. After stirring for 20 min and filtering the precipitate, the remaining arsenic concentrations were measured by AAS, 630 Shimadzu. Figure 7 shows the dependence of the remaining arsenic concentration as a function of the pH level of the solution. It can be seen that when the pH level of the solution was from 5 to 8, the arsenic adsorption was better. When the pH was higher than 12, the arsenic adsorption capacity of material is decreased clearly. Especially for the pH of 14, the sample did not adsorb As. The dependence of arsenic adsorption capacity on the pH level of solution can be explained by the different dissociation ability of As(III) corresponding to each different pH values in water and decomposition state of adsorbent. Easy to see that the arsenic adsorption of material M_1 is stronger than that of Fe_3O_4 and even PNA non-magnetic materials (M_0) also adsorb arsenic at the pH

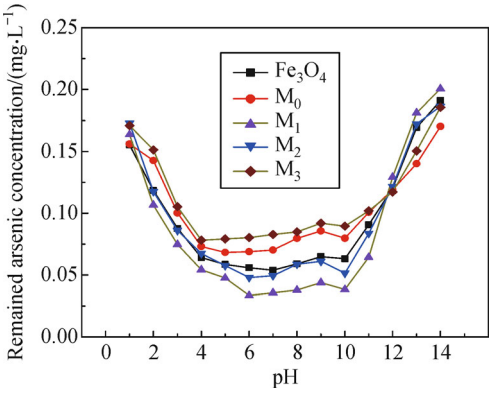

Fig. 7 Dependence of the remained arsenic concentration as a function of the pH.

level of solution from 5 to 8. When pH is about 7, the influence of pH on the arsenic adsorption capacity can also be caused by an oxidation state of PNA (original υ_{C-N^+}). Thus, it has the contribution of electrostatic affinity interaction between the materials to creating As(III) anion adsorption. At a high pH, As(III) exists as $H_2AsO_3^-$ and $HAsO_3^{2-}$ anions, simultaneously the surface of the nanoparticles is negatively charged. On the other hand, the surface charges appeared on the surface of nanoparticles, and they push anions in the solution. Thus, the adsorption process decreases with the corresponding increase of the pH level. Especially at pH = 14, due to a large electrostatic repulsion, the material has no arsenic adsorption capacity.

In the environment with pH < 5, the adsorption material can be decomposed a part, so the adsorption of the material is decreased. For this investigations, the sample amounts of 1 g of Fe_3O_4 are added to 100 mL solutions with pH = 1 and 2, respectively, after that they are stirred for 20 min. After filtering the precipitations, the dissolved iron ion concentration in solution is measured by an atomic absorption spectroscopy. The results showed that the reaction between Fe_3O_4 and the acid created the dissolved iron ions in solution with Fe concentration of 0.21 ppb (for pH = 1), and 0.13 ppb (for pH = 2), respectively. However, the iron ions did not appear in the solution of pH = 7. Although the decomposition of Fe_3O_4 is small, it is attributed to the low arsenic adsorption in the pH < 5. Meanwhile, this material is quite stable in neutral environment because no appearance of iron ions in solution of pH = 7. From the results in Fig. 7, it can be seen that Fe_3O_4 is also stable in alkaline environment of pH = 14. So these findings suggest the de-adsorption method in a solution of pH = 14 to reuse the adsorbent in many times.

3.4.2 Adsorption equilibrium time

Adsorption equilibrium time was evaluated by measurements of remaining arsenic concentrations in solution pH 7 after each interval stir different (after 10, 15, 20, 25, 30, 50 min) for the Fe_3O_4, M_0, M_1, M_2 and M_3 adsorbents as shown in Fig. 8. The observed results showed that after 20 min stirring period, the remaining arsenic concentrations stay in equilibrium.

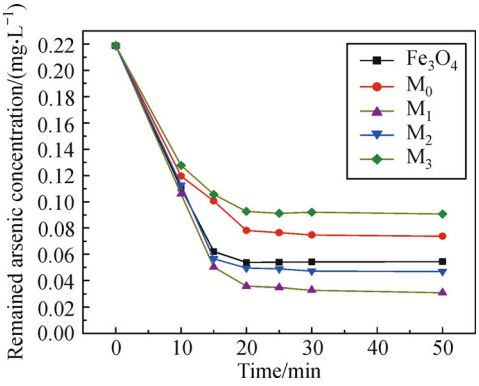

Fig. 8 Determination of equilibrium time of arsenic absorption.

3.4.3 Adsorption kinetic, specific surface area and porous properties of adsorbents

The experimental results and above analysis showed that the inelastic exchange interaction energy between the porous materials with high specific surface area of adsorption substance was occurred at the surface of nanoparticles, affecting mainly to their adsorption capacity. In order to thoroughly explain the nature of the As(III) treatment mechanism of nanoparticles, the nitrogen adsorption–desorption isotherms of typical samples (0.54 g of Fe_3O_4 and 0.54 g of M_1) at 77 K were studied in order to investigate the surface and mesopores structure of nanoparticles by the BET measurement [34] on TriStar 3000 V6.07 A equipment with TriStar 3000 V6.08 software. The adsorption hysteresis was observed in the region of a relative pressure $P/P_0 \approx 1$ (P_0 the saturation pressure of the nitrogen gas). The collision of nitrogen molecules with nanoparticles is taken to be inelastic, so that the nitrogen molecular remains in contact with the nanoparticles for a time before returning to the gas phase. This time delay is taken as responsible for the phenomenon of adsorption that demonstrated by equation [30] as follows:

$$\frac{P}{V_a(P_0-P)} = \frac{1}{V_m}\cdot\frac{P}{P_0} \quad (4)$$

where V_a is the quantity of gas adsorbed at pressure P, and V_m is the quantity of gas adsorbed when the entire surface is covered with a mono molecular layer. From the above analysis, the Langmuir model is appropriate for the arsenic adsorption in the pH = 7 environment that is similar to the nitrogen adsorption process of adsorbents at a temperature of 77 K. Thus the adsorbents were studied to examine their porosity and surface properties by the BET measured method [6–7,34] and the Langmuir isotherm equation.

The insets in Figs. 9 and 10 depict the nitrogen adsorption–desorption isotherm curves for typical Fe_3O_4 and M_1 samples, respectively. These hysteresis loops are attributed mesopore characteristic capillary condensation of nitrogen at standard conditions for temperature and pressure (STP) between nanoparticles of Fe_3O_4 and M_1. The adsorbed quantities standardized to convert become the characteristic quantities of porosity such as the cumulative pore volume (cm^3/g) and average pore size. The changes in slope of this hysteresis loop and its general shape gave a quick overview of how porosity was distributed in the samples. Figures 9 and 10 provide the fundamental means, in which the pore volume is concentrated and its distribution is characteristics through average pore size. The pore size distribution calculated by the BET method [10,34] at relative pressure $P/P_0 \approx 1$. From Figs. 9 and 10, the maximum absorption volumes (dV/dD *vs.* pore size range of D) belongs to pore size range of about 12–15 nm. The specific surface areas of samples calculated by the BET method are presented in Table 2.

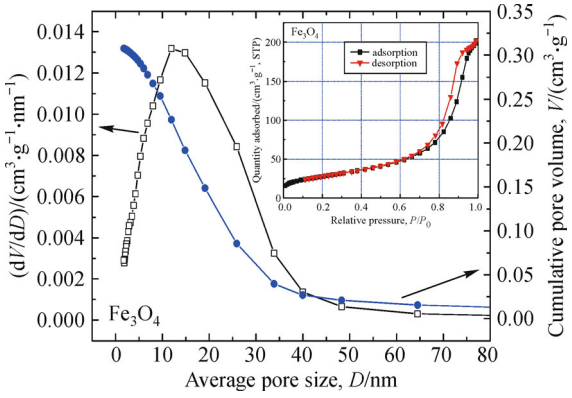

Fig. 9 The pore distribution is characteristics through average pore size of Fe_3O_4 sample (inset: the adsorption–desorption isotherm curve of N_2 at 77 K).

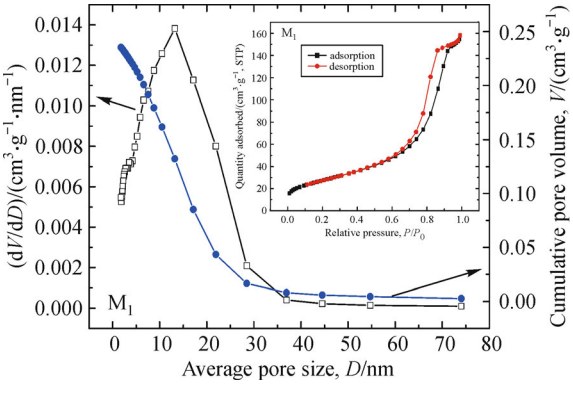

Fig. 10 The pore distribution is characteristics through average pore size of M_1 sample (inset: the adsorption–desorption isotherm curve of N_2 at 77 K).

Table 2 Specific surface area, saturate magnetic moment and maximum absorption capacity of Fe_3O_4, M_0, M_1, M_2 and M_3

Sample	BET specific surface area /($m^2\cdot g^{-1}$)	Saturate magnetic moment /(emu·g^{-1})	q_{max} /(mg·g^{-1})
Fe_3O_4	100.28	63.13	32.88
M_0	5.32	0.00	23.45
M_1	99.08	58.38	46.97
M_2	38.35	56.73	37.74
M_3	43.06	43.43	20.27

3.4.4 Maximum arsenic adsorption capacity

In order to determine the arsenic adsorption capacity of nanopowders in the pH = 7 environment, the adsorbent material of 0.01 g was used to adsorb the arsenic in 100 mL solutions with initial arsenic concentrations of 150 ppb maintained at pH = 7. After stirring for 20 min and filtering the precipitate, the remaining arsenic concentrations (in ppb) were measured by AAS. From the above analysis, the Langmuir model is appropriate for the arsenic adsorption in the pH = 7 environment that is similar to the nitrogen adsorption process of adsorbents at a temperature of 77 K. Thus, the maximum arsenic adsorption capacity q_{max} corresponding to a unit volume of adsorbent (mg/g) is calculated by the Langmuir isotherm equation in equilibrium point at pH = 7 and 300 K [6,10,17]:

$$\frac{C_f}{q} = \left(\frac{1}{q_{max}}\right)C_f + \frac{1}{bq_{max}} \quad (5)$$

The form of graphs is $y = ax + c$, with $y = C_f/q$, $x = C_f$, $a = 1/q_{max}$, $c = 1/(bq_{max})$. Among them, C_f is the remaining arsenic concentration (mg/L) at equilibrium was measured on AAS, q is the arsenic adsorption capacity at equilibrium corresponding to a unit volume of adsorbent (mg/g), and b is the constant characterizing the interaction of the adsorbent and adsorbed substances.

The dependence of C_f/q on C_f is shown in Fig. 11. From

these plots, the calculated values of q_{max} for Fe_3O_4, M_0, M_1, M_2 and M_3 are presented in Table 2.

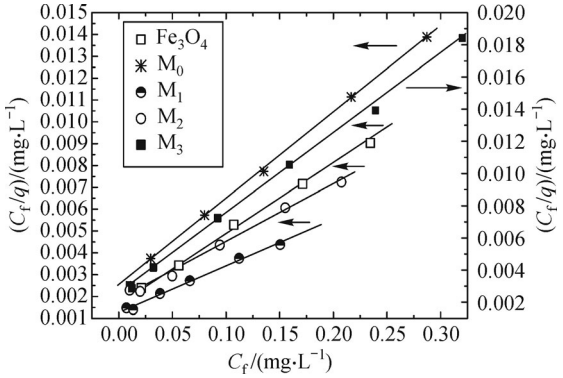

Fig. 11 The Langmuir adsorption isotherm curves.

Although, the saturation magnetic moment and the specific surface area of PNA/Fe_3O_4 decreased with the increase of the polymer concentration, Table 3 shows the arsenic adsorption capacity of materials to be sorted in the order M_1, M_2, Fe_3O_4, M_0 and M_3, in which q_{max} of the M_1 material is larger than that of Fe_3O_4 and the results in Ref. [6] in the same conditions at pH 7. The results in Table 3 are also fit well with the experimental results shown in Fig. 8 with the pH = 7 solution.

Table 3 Soluble iron ion concentration in the HCl solution

pH	Soluble iron ion concentration /ppb	
	Fe_3O_4	M_3
1	0.21	0.17
2	0.13	0.13
7	–	–

However, the polymer shell contributed to the chemical stabilization of Fe_3O_4 cores, so the magnetic moment of samples is stable over time. Besides, Table 2 shows that the non-magnetic nanomaterial (M_0 sample) with the specific surface area 5.32 m^2/g also absorbed arsenic with q_{max} = 23.45 mg/g.

This issue proved the contribution of PNA to the arsenic adsorption capacity in solution. When pH ≈ 7, the influence of pH on the absorption capacity of arsenic can also be caused by the oxidation state of PNA (original υ_{C-N^+}), and it has the contribution of affinity electrostatic interactions between nanoparticles, creating anions adsorbed As(III). When the solution with a high pH (e.g., pH = 14, in Fig. 7), arsenic is less adsorbed by the absorbents. This can be explained by the high pH (at pH > 10) PNA converted from the oxidation state to deoxidize state, so the interactions between the absorbents and the anion As(III) in the form of $H_2AsO_3^-$ and $HAsO_3^{2-}$ were decreased markedly (Fig. 7). In pH < 5 the adsorption of material may decrease by the decomposition in part of materials in highly acidic environments. To investigate the decomposition of absorbents, the amounts of 1 g of Fe_3O_4 and M_3 of samples is added to 100 mL of HCl with pH = 1 and 2 and stirred for 20 min. After filtering the precipitate, the soluble iron ion concentrations in the HCl solution were examined by AAS Shimadzu 6300 and were calculated as shown in Table 3.

Although the decompositions of Fe_3O_4 and PNA/Fe_3O_4 composite were small, they can also decrease the arsenic adsorption capacity in the environment with pH < 5.

Meantime, the appearance of iron ions do not see in solution with pH ⩾ 7, this issue proved quite durable materials in a neutral and alkaline environment. In alkaline medium, Fe_3O_4 and the composite materials of PNA/Fe_3O_4 are fairly stable, so the above results suggest the desorption method in solution pH = 14 to reuse the adsorbents in many times.

4 Conclusions

The PNA/Fe_3O_4 nanocomposite materials have been successfully synthesized with different polymer concentrations. The PNA/Fe_3O_4 nanoparticles are capable of As(III) adsorption, but the arsenic adsorption capacity of M_1 nanocomposite is better than Fe_3O_4. The optimal conditions for As(III) adsorption is pH ≈ 7 and the adsorption time is 20 min. The dynamics of arsenic adsorption is explained on the basis of the BET method and the Langmuir isotherm adsorption on the surface of porous nanomaterials. In an environment with pH > 14, these materials could be reabsorbed and reused.

Abbreviations

AAS	atomic absorption spectroscopy
BET	Brunauer–Emmett–Teller
IOCD	iron oxide-coated diatomite
IOCS	iron oxide-coated sand
PNA	poly(1-naphthylamine)
SEM	scanning electron microscopy
STP	standard conditions for temperature and pressure
TEM	transmission electron microscopy
VSM	vibrating sample magnetometer
XRD	X-ray diffraction

Acknowledgements This work was supported by the NAFOSTED Foundation, Code: 103.02-2013.49.

References

[1] Shah P, Sohma M, Kawaguchi K, et al. Growth conditions, structural and magnetic properties of M/Fe_3O_4/I (M = Al, Ag and I = Al_2O_3, MgO) multilayers. Journal of Magnetic and Materials, 2002, 247(1): 1–5

[2] Liu J, Bin Y, Matsuo M. Magnetic behavior of Zn-doped Fe_3O_4 nanoparticles estimated in terms of crystal domain size. Journal of Physical Chemistry C, 2012, 116(1): 134–143

[3] Bertone J F, Cizeron J, Wahi R K, et al. Hydrothermal synthesis of quartz nanocrystal. Nano Letters, 2003, 3(5): 655–659

[4] Rusanov A I. Surface thermodynamic revisited. Surface Science Reports, 2005, 58(5–8): 111–239

[5] Gu H, Huang Y, Zhang X, et al. Magnetoresistive polyaniline-magnetite nanocomposites with negative dielectrical properties. Polymer, 2012, 53(3): 801–809

[6] Khodabakhshi A, Amin M M, Mozaffari M. Synthesis of magnetic nanoparticles and evaluation of its efficiency for arsenic removal from simulated industrial wastewater. Iranian Journal of Environmental Health Sciences & Engineering, 2011, 8(3): 189–200

[7] Auffan M, Rose J, Proux O, et al. Enhanced adsorption of arsenic onto magnetic nanoparticles: As(III) as a probe of surface structure and heterogeneity. Langmuir, 2008, 24(7): 3215–3222

[8] Zouboulis A I, Katsoyiannis I A. Recent advances in the bioremediation of arsenic-contaminated groundwaters. Environment International, 2005, 31(2): 213–219

[9] Chaudhary G R, Saharan P, Kumar A, et al. Adsorption studies of cationic, anionic and azo-dyes via monodispersed Fe_3O_4 nanoparticles. Journal of Nanoscience and Nanotechnology, 2013, 13 (5): 3240–3245

[10] Liu R, Lu Y, Shen X, et al. Adsorption kinetics and isotherms of arsenic(V) from aqueous solution onto $Ni_{0.5}Zn_{0.5}Fe_2O_4$ nanoparticles. Journal of Nanoscience and Nanotechnology, 2013, 13(4): 2835–2841

[11] Fang X B, Fang Z Q, Tsang P K E, et al. Selective adsorption of Cr (VI) from aqueous solution by EDA-Fe_3O_4 nanoparticles prepared from steel pickling waste liquor. Applied Surface Science, 2014, 314: 655–662

[12] Hao T, Yang C, Rao X, et al. Facile additive-free synthesis of iron oxide nanoparticles for efficient adsorptive removal of Congo red and Cr(VI). Applied Surface Science, 2014, 292: 174–180

[13] Yang G, Tang L, Lei X, et al. Cd(II) removal from aqueous solution by adsorption on α-ketoglutaric acid-modified magnetic chitosan. Applied Surface Science, 2014, 292: 710–716

[14] Chen Q, He Q, Lv M, et al. The vital role of PANI for the enhanced photocatalytic activity of magnetically recyclable N–$K_2Ti_4O_9$/$MnFe_2O_4$/PANI composites. Applied Surface Science, 2014, 311: 230–238

[15] Jiang Q L, Zheng S W, Hong R Y, et al. Folic acid-conjugated Fe_3O_4 magnetic nanoparticles for hyperthermia and MRI *in vitro* and *in vivo*. Applied Surface Science, 2014, 307: 24–233

[16] Chen M J, Shen H, Li X, et al. Facile synthesis of oil-soluble Fe_3O_4 nanoparticles based on a phase transfer mechanism. Applied Surface Science, 2014, 307: 306–310

[17] Babu C M, Palanisamy B, Sundaravel B, et al. A novel magnetic Fe_3O_4/SiO_2 core–shell nanorods for the removal of arsenic. Journal of Nanoscience and Nanotechnology, 2013, 13(4): 2517–2527

[18] Chen L, Xin H, Fang Y, et al. Application of metal oxide heterostructures in arsenic removal from contaminated water. Journal of Nanomaterials, 2014, 793610 (10 pages)

[19] Park J W, Jang A N, Song J H, et al. Electronic structure of Zn doped Fe_3O_4 thin films. Journal of Nanoscience and Nanotechnology, 2013, 13(3): 1895–1898

[20] Li X, Zhang F, Ma C, et al. Green synthesis of uniform magnetite (Fe_3O_4) nanoparticles and micron cubes. Journal of Nanoscience and Nanotechnology, 2012, 12(3): 2939–2942

[21] Zapotoczny B, Dudek M R, Guskos N, et al. FMR study of the porous silicate glasses with Fe_3O_4 magnetic nanoparticles fillers. Journal of Nanomaterials, 2012, 341073 (7 pages)

[22] Méndez-Rodríguez L, Zenteno-Savín T, Acosta-Vargas B, et al. Differences in arsenic, molybdenum, barium, and other physico-chemical relationships in groundwater between sites with and without mining activities. Natural Science, 2013, 5(2): 238–243

[23] Lin K S, Dehvari K, Liu Y J, et al. Synthesis and characterization of porous zero-valent iron nanoparticles for remediation of chromium-contaminated wastewater. Journal of Nanoscience and Nanotechnology, 2013, 13(4): 2675–2681

[24] Zaki H M, Al-Heniti S, Umar A, et al. Magnesium-zinc ferrite nanoparticles: effect of copper doping on the structural, electrical and magnetic properties. Journal of Nanoscience and Nanotechnology, 2013, 13(6): 4056–4065

[25] Larumbe S, Gómez-Polo C, Pérez-Landazábal J I, et al. Ni doped Fe_3O_4 magnetic nanoparticles. Journal of Nanoscience and Nanotechnology, 2012, 12(3): 2652–2660

[26] Rathore D, Kurchania R, Pandey R K. Structural, magnetic and dielectric properties of $Ni_{1-x}Zn_xFe_2O_4$ (x = 0, 0.5 and 1) nanoparticles synthesized by chemical co-precipitation method. Journal of Nanoscience and Nanotechnology, 2013, 13(3): 1812–1819

[27] Liu X, Zhong Z, Tang Y, et al. Review on the synthesis and applications of Fe_3O_4 nanomaterials. Journal of Nanomaterials, 2013, 902538 (7 pages)

[28] Abdallah H M, Moyo T. Evidence of superparamagnetism in $Mg_{0.5}Mn_{0.5}Fe_2O_4$ nanosized ferrite. Journal of Superconductivity and Novel Magnetism, 2015, 28(3): 955–960

[29] Genç F, Turhan E, Kavas H, et al. Magnetic and microwave absorption properties of $Ni_xZn_{0.9-x}Mn_{0.1}Fe_2O_4$ prepared by boron addition. Journal of Superconductivity and Novel Magnetism, 2015, 28(3): 1047–1050

[30] Uwamariya V, Petrusevski B, Slokar Y M, et al. Effect of fulvic acid on adsorptive removal of Cr(VI) and As(V) from groundwater by iron oxide-based adsorbents. Water, Air, and Soil Pollution, 2015, 226(6): 184

[31] Fakour H, Pan Y F, Lin T F. Effect of humic acid on arsenic adsorption and pore. blockage on iron-based adsorbent. Water, Air, and Soil Pollution, 2015, 226(2): 14

[32] Ameen S, Akhtar M S, Umar A, et al. Effective modified electrode of poly(1-naphthylamine) nanoglobules for ultra-high sensitive ethanol chemical sensor. Chemical Engineering Journal, 2013, 229: 267–275

[33] Ameen S, Akhtar M S, Kim Y S, et al. Synthesis and characterization of novel poly(1-naphthylamine)/zinc oxide nanocomposites: Application in catalytic degradation of methylene blue dye. Colloid & Polymer Science, 2010, 288(16–17): 1633–1638

[34] Webb P A, Orr C, Camp R W, et al. Analytical Methods in Fine Particle Technology. Norcross, GA, USA: Micromeritics Instrument Corporation, 1997, 60–62